

Improving competitive evacuations with a vestibule structure designed from panel-like obstacles

I.M. Sticco^a, G.A. Frank^b, C.O. Dorso^{a,c}

^a*Departamento de Física, Facultad de Ciencias Exactas y Naturales, Universidad de Buenos Aires, Pabellón I, Ciudad Universitaria, 1428 Buenos Aires, Argentina.*

^b*Unidad de Investigación y Desarrollo de las Ingenierías, Universidad Tecnológica Nacional, Facultad Regional Buenos Aires, Av. Medrano 951, 1179 Buenos Aires, Argentina.*

^c*Instituto de Física de Buenos Aires, Pabellón I, Ciudad Universitaria, 1428 Buenos Aires, Argentina.*

Abstract

It has been shown that placing an obstacle in front of an exit door has proven to be a successful method to improve pedestrian evacuations. In this work, we will focus on the space limited by the exit and the obstacles (*i.e.* the vestibule structure). We analyzed two different types of vestibules: the two-entry vestibule (which consists of a single panel-like obstacle) and the three-entry vestibule (which consists of two panel-like obstacles). In the former, we studied the effects of varying the walls' friction coefficient κ_w and the distance from the obstacle to the exit door d . In the latter, we varied the space between the two panels (*gap*). We found that the three above mentioned parameters control the vestibule's density, which subsequently affects the evacuation flow (fundamental diagram). We have also found that reducing the distance d or increasing the friction facilitates the formation of blocking clusters at the vestibule entries, and hence, diminishes the density. If the density is too large or too low, the evacuation flow is suboptimal, whereas if the density is around 2 p/m^2 , the flow is maximized. Our most important result is that the density (and therefore the evacuation flow) can be precisely controlled by κ_w , d , and the *gap*. Moreover, the three-entry vestibule produced the highest evacuation flow for specific configurations of the *gap* and the distance from the panels to the door.

Keywords: Pedestrian evacuation, panel-like obstacle, vestibule.

1. Introduction

The counterintuitive effect that an obstacle in front of a door can improve the performance of pedestrian evacuation is receiving more attention every year. This novel assessment was suggested for the first time in the same paper where the escape panic version of the social force model was introduced [1]. From that time, many studies have been conducted to exploit this phenomenon at its most.

Escobar & De la Rosa performed numerical simulations using the escape panic version of the social force model to simulate pedestrian evacuations [2]. They tested the performance of several architectural layouts in terms of the evacuation flow. They reported the existence of the “waiting room effect”. The waiting room (also known as “vestibule” in the architecture jargon [3]) is the space in between the obstacles and the exit door, and its associated effect is the flow improvement whenever the inflow to this room does not exceed the outflow.

The first experiment of pedestrian evacuation using a column-like obstacle appeared in Ref. [4] (to our knowledge). Although the number of participants was small ($N = 20$), the results are qualitatively consistent with the previous numerical simulations. Frank & Dorso performed numerical simulations of evacuations using panel-like obstacles [5]. They show that, under certain conditions, the panel-like obstacles may exceed the performance of pillar-like obstacles. They also report the “clever is not always better” effect, meaning that the overall evacuation may be improved if the agents follow a non-strategic plan in order to avoid the obstacles.

Although most of the investigations focused on the pillar-like obstacle [6, 7, 8, 9, 10], the panel-like obstacle appears to perform better in the evacuation process, and thus, has brought the interest in the last years [5, 11, 12]. The first

laboratory experiment using a panel-like obstacle was performed by Haghani & Savri [13]. Under certain experimental conditions, they found that the panel improves the evacuation if the doors are narrow enough.

Ref. [11], performed a numerical optimization for the dimensions and location of panel-like and pillar-like obstacles. They claim that the former perform better than the latter because of the capability to reduce the egress time and the pressure among pedestrians. They emphasize that these conclusions hold even for a wide set of parameters. A more recent investigation carried out by the same group, experimentally confirms that panels yield better performance than the pillars [14].

Although most of the researches state that the panel-like obstacle improves the evacuation, other novel results challenge this statement [15]. For instance, a recent study explores the limitations of the panel-like obstacle when the pedestrians face a limited-visibility situation [12].

For a complete review on the obstacle effects in many diverse systems, (including cellular automata [16, 17, 18]), see Ref. [19]. It should be mentioned that the interest in the obstacle's effect went beyond the pedestrian dynamics field since it has been further explored in granular media [20, 21, 22] and bottleneck egress with animals [23, 24, 25].

One of the most common ways to quantify the capacity of a pedestrian facility is by means of the fundamental diagram. That is, the flow-density relation (or velocity-density relation) [26]. The fundamental diagram exhibits two different regimens: the free-flow regime, in which the flow increases as the density increases, and the congested regime, in which the flow decreases as the density increases. The fundamental diagram has been studied in many contexts ranging from laboratory conditions [26, 27, 28] to real-life situations [29, 30]. A more detailed insight into this topic can be found in Refs. [31, 32, 33].

The fundamental diagram at bottlenecks is still a subject of debate due to the lack of consensus on the expected regimes. Kuperman et al., for instance, performed a controlled experiment where they measured the egress flow as a function of the pedestrian density close to the exit door [34]. Contrary to expected results, they report an increasing flow even for density values as high as $\rho = 9 \text{ p/m}^2$.

Ref. [35], obtained the fundamental diagram of a real-life earthquake evacuation. Although the density values did not exceed $\rho = 6 \text{ p/m}^2$, they found a non-monotonically flow increment versus density. On the other hand, the laboratory experiments appearing in Ref. [36] exhibit a plateau in the flow after the capacity (the maximum flow) is achieved. Nevertheless, other laboratory experiments in bottleneck environments display the typical flow diminution that characterizes the congested regime [37, 38].

The discrepancy across the literature results may be attributed to the differences in the door's width, the disparity in the participants' anxiety level and the variation between measurement areas (among other reasons). It should be mentioned, though, that the fundamental diagram is highly sensible to the flow measurement criteria as thoroughly analyzed in Ref. [39]. Another consideration to take into account is that controlled experiments are not suitable for reproducing panic conditions since participants are not allowed to harm each other (due to safety reasons).

It is worth mentioning that the link between the flow-density relation and pedestrian evacuations in the presence of obstacles is almost unexplored [40]. In this paper, we will bridge the gap between the fundamental diagram and the evacuations in the presence of panel-like obstacles.

2. Background

2.1. The Social Force Model

The social force model [1] provides a necessary framework for simulating the collective dynamics of pedestrians (*i.e.* self-driven agents). The pedestrians are represented as simulated agents that follow an equation of motion involving either “socio-psychological” forces and physical forces. The equation of motion for any agent i of mass m_i reads

$$m_i \frac{d\mathbf{v}_i}{dt} = \mathbf{f}_d^{(i)} + \sum_{j=1}^N \mathbf{f}_s^{(ij)} + \sum_{j=1}^N \mathbf{f}_p^{(ij)} \quad (1)$$

where the subscript j corresponds to any neighboring agent or the walls. The three forces \mathbf{f}_d , \mathbf{f}_s and \mathbf{f}_p are different in nature. The desire force \mathbf{f}_d represents the acceleration of a pedestrian due to his/her own will. The social force \mathbf{f}_s , instead, describes the tendency of the pedestrians to stay away from each other (social distancing). The physical force \mathbf{f}_p stands for both the sliding friction and the repulsive body force.

The pedestrians’ own will is modeled by the desire force \mathbf{f}_d . This force stands for the acceleration required to move at the desired walking speed v_d . The parameter τ reflects the reaction time. Thus, the desire force is modeled as follows

$$\mathbf{f}_d^{(i)} = m \frac{v_d^{(i)} \hat{\mathbf{e}}_d^{(i)}(t) - \mathbf{v}^{(i)}(t)}{\tau} \quad (2)$$

where $\hat{\mathbf{e}}(t)$ represents the unit vector pointing to the target position and $\mathbf{v}(t)$ stands for the agent velocity at time t .

The tendency of any individual to preserve his/her personal space is accomplished by the social force \mathbf{f}_s . This force is expected to prevent the agents from getting too close to each other (or to the walls) in any environment. The model

for this kind of “socio-psychological” behavior is as follows

$$\mathbf{f}_s^{(i)} = A e^{(R_{ij}-r_{ij})/B} \hat{\mathbf{n}}_{ij} \quad (3)$$

where r_{ij} means the distance between the center of mass of the agents i and j , and $R_{ij} = R_i + R_j$ is the sum of the pedestrians radius. The unit vector $\hat{\mathbf{n}}_{ij}$ points from pedestrian j to pedestrian i , meaning a repulsive interaction. The parameter B is a characteristic scale that plays the role of a fall-off length within the social repulsion. At the same time, the parameter A represents the intensity of the social repulsion.

The expression for the physical force (the friction force plus the body force) has been inspired from the granular matter field [41]. The mathematical expression reads as follows

$$\mathbf{f}_p^{(ij)} = \kappa_t g(R_{ij} - r_{ij}) (\Delta \mathbf{v}^{(ij)} \cdot \hat{\mathbf{t}}_{ij}) \hat{\mathbf{t}}_{ij} + k_n g(R_{ij} - r_{ij}) \hat{\mathbf{n}}_{ij} \quad (4)$$

where $g(R_{ij} - r_{ij})$ equals $R_{ij} - r_{ij}$ if $R_{ij} > r_{ij}$ and vanishes otherwise. $\Delta \mathbf{v}^{(ij)} \cdot \hat{\mathbf{t}}_{ij}$ represents the relative tangential velocities of the sliding bodies (or between the individual and the walls).

The sliding friction occurs in the tangential direction while the body force occurs in the normal direction. Both are assumed to be linear with respect to the net distance between contacting agents. The sliding friction is also linearly related to the difference between the tangential velocities. The coefficients κ_t (for the sliding friction) and k_n (for the body force) are related to the contacting surfaces materials and the body stiffness, respectively.

The model parameter values were chosen to be the same as the best-fitting parameters reported in the recent study from Ref. [42] These values were obtained by fitting the model to a real-life event that resemblances an emergency evacuation. The parameter values are: $A = 2000$ N, $B = 0.08$ m, $\kappa_t =$

$3.05 \times 10^5 \text{ kg}/(\text{m}\cdot\text{s})$, $k_n = 3600 \text{ N/m}$, $\tau = 0.5 \text{ s}$.

The friction force between an agent and a wall has the same mathematical expression as the friction between two agents. Nevertheless, we distinguish the friction coefficient between agents κ_t and the wall friction coefficient κ_w . In this paper, we will fix the value of κ_t , but we will explore different values of κ_w .

2.2. Blocking clusters

A characteristic feature of pedestrian dynamics is the formation of clusters. Clusters of pedestrians can be defined as the set of individuals that for any member of the group (say, i) there exists at least another member belonging to the same group (j) in contact with the former. Thus, we define a “granular cluster” (C_g) following the mathematical formula given in Ref. [43]

$$C_g : P_i \in C_g \Leftrightarrow \exists j \in C_g / r_{ij} < (R_i + R_j) \quad (5)$$

where (P_i) indicate the i th pedestrian and R_i is his/her radius (half of the shoulder width). That means, C_g is a set of pedestrians that interact not only with the social force, but also with physical forces (*i.e.* friction force and body force). A “blocking cluster” is defined as the minimal granular cluster which is closest to the door whose first and last agents are in contact with the walls at both sides of the door [44]. Previous studies have demonstrated that the blocking clusters play a crucial role in preventing pedestrians from getting through a door [44, 45, 46].

3. Numerical simulations

We carried out our investigation by performing numerical simulations of pedestrians evacuating a room in the presence of one or two obstacles, as it is shown in Fig. 1. We simulated a crowd of $N = 200$ agents whose trajectories followed a classical Newton equation of motion. We used the escape panic

version of the social force model for the interaction forces acting on the agents (see Section 2.1 for the mathematical expressions). The model parameter values were chosen to be the same as the best-fitting parameters reported in the recent study from Ref. [42], the values were introduced in Section 2.1.

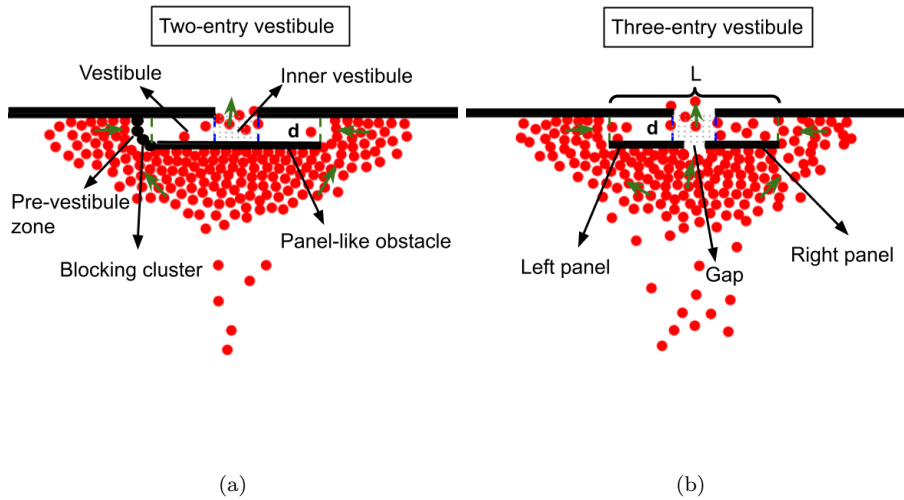


Figure 1: Visual representations of the numerical simulations, the red circles represent the agents. The space between the obstacle and the walls is the vestibule (delimited by green vertical dashed lines). The letter ‘d’ on the vestibule denotes the vertical distance between the panels and the door. The “inner vestibule” is the dotted area enclosed by vertical blue lines (close to the exit door). The green arrows stand for the desired velocity. **(a)** Two-entry vestibule structure. The black agents located at the left entrance to the vestibule make up a blocking cluster in the pre-vestibule zone. **(b)** Three-entry vestibule structure.

The mass of the agents was fixed at $m = 80$ kg, and the radius was set to $R = 0.23$ m according to the data from Ref. [47]. The desired velocity (which is the parameter that controls the anxiety level) was varied in the interval $0.5 \text{ m/s} \leq v_d \leq 6 \text{ m/s}$. The upper limit ($v_d = 6 \text{ m/s}$) is a velocity high enough to represent a rush but low enough to be achieved by non-professional runners [48]. Initially, the agents were placed in a $20 \text{ m} \times 20 \text{ m}$ area with random positions and velocities. The direction of the desired velocity was such that the agents located outside the vestibule point to the vestibule through the nearest

entry. Once they were inside the vestibule, the target became the exit door (see the green arrows in Fig. 1).

The exit door’s size was $DS = 1.84$ m, which is equivalent to four agents’ diameter in accordance to Ref. [42]. The two-entry vestibule (Fig. 1a) has a single unidimensional panel of size $L = 4 \times DS = 7.36$ m centered with respect to the door (in the same way as in Ref. [5]). Notice that it is possible to access the vestibule from the left or right sides (these are the two-entries).

The three-entry vestibule (Fig. 1b) has two panels of the same size. We call it “three-entry” because the gap between panels becomes the third entry (in addition to the left and right entries). The *gap* is defined as the space between panels. The size of the panels was constrained by the gap between them. The distance between the ends of the panels was fixed at $L = 7.36$ m (see Fig. 1b).

We analyzed the effect of varying four parameters: the desired velocity v_d , the wall friction coefficient κ_w , the vertical distance between the obstacle and the door d and, in the case of the three-entry vestibule, we varied the gap between panels (*gap*). We stress that the wall friction coefficient is also the panel’s friction coefficient since, in this paper, panels are treated as walls. It should be noted that the three parameters are architectural features that could be easily handled by designers and contractors.

For each parameter configuration, we performed 30 evacuation processes that finished when 90% of agents left the room. No re-enter of agents was allowed. We measured the mean density, the evacuation flow, and the probability of blocking clusters. The mean density was measured in the inner vestibule region. It was defined as the number of agents divided by the corresponding occupied area. The evacuation flow was defined as the the number of evacuated agents divided by the evacuation time. The blocking clusters are the set of pedestrians that block a door (see Section 2.2 for a formal definition). We

measured the probability of attaining blocking clusters at the entries of the two-entry vestibule (at the pre-vestibule zone). The probability was defined as the fraction of time with blocking clusters over the total evacuation time.

The numerical simulations were carried out using LAMMPS, which is a molecular dynamics open-access software [49]. The implementation also required customized modules developed in C++. The integration of the agents' trajectory was calculated using the Velocity Verlet algorithm with a time-step $\Delta t = 10^{-4}$ s.

3.1. Clarifications

In order to keep this paper concise and clear, we will only report the results corresponding to the numerical simulations described above. Nevertheless, we want to mention that we performed numerical simulations with higher number of agents $N = 400$ (instead of $N = 200$) and we obtained similar qualitative results to the ones that will be reported in Section 4. We also tested the results' robustness by replacing the unidimensional panels with obstacles of width $w = 0.12$ m [5] and no significant differences were observed.

We measured the density in the inner vestibule and the density in the whole vestibule (see Fig. 1). In both cases, the mean values are qualitatively similar. This paper only reports the results corresponding to the inner vestibule density because the data exhibit less dispersion around the mean values.

For simplicity reasons, we will omit the units of friction coefficient κ_w . Bear in mind that its units are kg/(m.s). The gap between panels will be expressed in units of agents' diameter. In this context, we will use the letter 'p' to refer to the agent diameter. For instance, $gap = 3$ p means that the gap size is $gap = 3 \times 0.46$ m (since the agent diameter is 0.46 m). The distance between the panel and the door d will be presented like in the following example: $d = 0.92$ m

(2p), where ‘2p’ stands for two agents’ diameter.

4. Results and discussions

We present in this Section the main results of our investigation. We divided this Section into three parts. In the first part (Sec. 4.1), we show the evacuation flow as a function of the desired velocity for both the two-entry vestibule and the three-entry vestibule.

In the following two parts, we explore only the highest desired velocity $v_d = 6$ m/s because this desired velocity corresponds to an anxious crowd that could lead to a dangerous situation. In Section 4.2 we present the results of the two-entry vestibule and the effects of varying either the friction of the walls and the distance of the obstacle to the door. In Section 4.3, we explore the consequences of placing two panel-like obstacles in front of the door (*i.e.* a three-entry vestibule) and the effects produced by varying the gap between the panels.

4.1. Flow vs. desired velocity

In this Section, we show results corresponding to both the two-entry vestibule and the three-entry vestibule. We will show the consequences on the flow after varying the desired velocity and the obstacle’s size. The desired velocity is the parameter that controls the pedestrians’ anxiety level. If the desired velocity is low (say, $v_d = 1$ m/s), it means that pedestrians are in a relaxed situation. On the other hand, a higher desired velocity (say, $v_d = 6$ m/s) means that pedestrians rush to exit the room.

Fig. 2 shows the evacuation flow as a function of the desired velocity for the two-entry vestibule. The flow is defined as $J = n/t_e$ where n is the number of

evacuated pedestrians and t_e is the time it takes to evacuate those n pedestrians. We show four “subplots”, each of them corresponds to different distances between the panel and the exit door (see the plots’ titles). Each curve is associated with a particular wall friction coefficient κ_w . We set $\kappa_w = 0$ as a limiting case where no wall friction is present, $\kappa_w = 3.05 \times 10^5$ corresponding to the value obtained from the optimization of parameters in Ref. [42] and $\kappa_w = 3.05 \times 10^6$ as the upper limit friction value explored in this research.

We explored four different conditions: the “no-vestibule” situation and the vestibule situation with three different wall friction values shown in the legends.

As a general feature, we observe that if the desired velocity is low ($v_d < 4$ m/s *i.e.* almost relaxed situation), the scenario without vestibule produces higher evacuation flows than the scenarios that includes it. Nevertheless, if the desired velocity is high enough ($v_d \geq 4$ m/s say, when the multitude is anxious and the risk of fatalities is present), the vestibule improves the evacuation performance for panels placed at $d = 1.38$ m and $d = 1.84$ m; see Figs. 2b and 2c in the range $v_d \geq 4$ m/s.

We measured the evacuation flow as a function of v_d for the three-entry vestibule structure. Fig. 3 shows the results corresponding to different distances between the panels and the exit door (see the plots’ titles). In this case, we varied the gap between the panels as shown in the legends.

We may conclude, from this Section, that the vestibule improves the evacuation performance (in terms of the evacuation flow) if the desired velocity is high enough (and within the explored range). This suggests that the vestibule structure may facilitate the egress of pedestrians if they feel a sudden urge to escape from a particular place (such as in an emergency evacuation). In the following two Sections, we set the desired velocity to $v_d = 6$ m/s. This value was chosen because it is high enough to ensure a high anxiety level but low enough

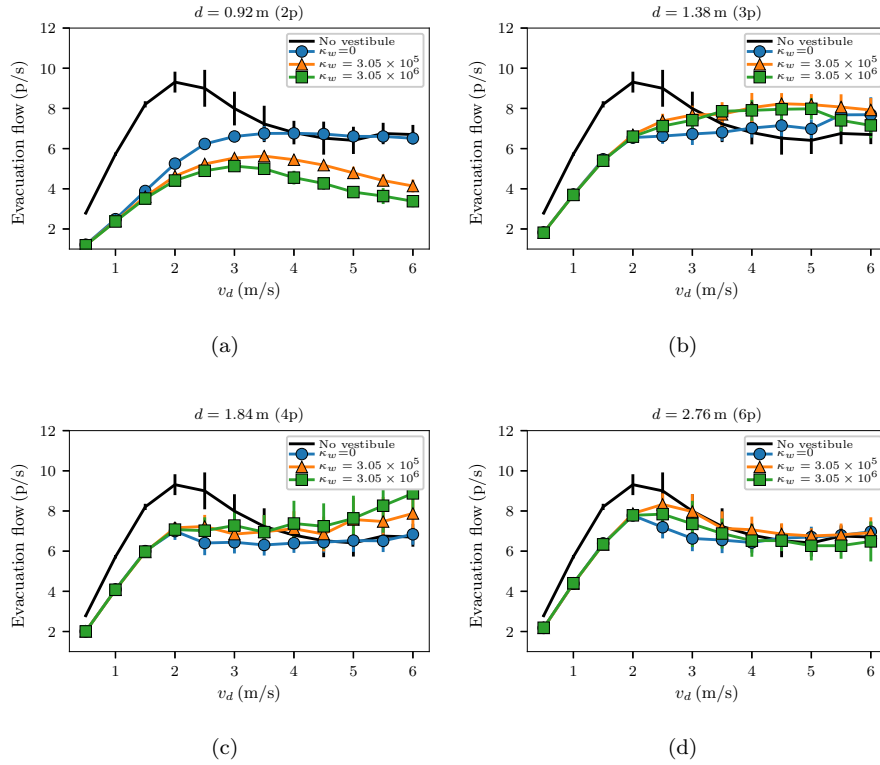


Figure 2: Evacuation flow as a function of the desired velocity for two-entry vestibules. The measurements are averaged over 30 evacuation processes where the initial positions and velocities were set at random. The initial number of pedestrians was $N = 200$. See the plot's title for the corresponding distance from the obstacle to the door. See the legend for the wall friction coefficient value κ_w .

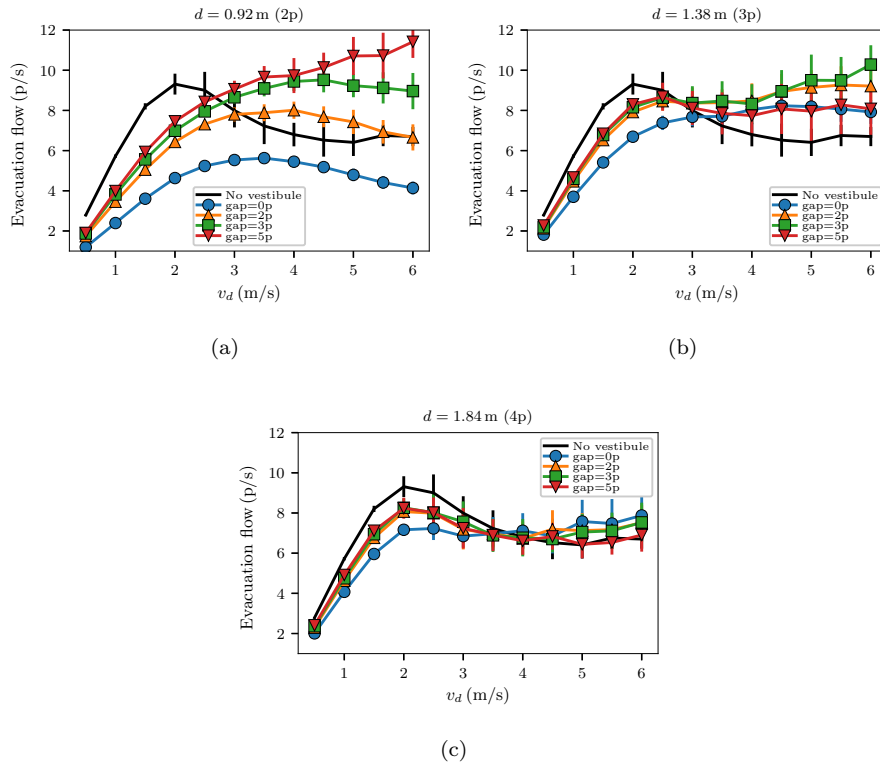


Figure 3: Evacuation flow as a function of the desired velocity for three-entry vestibules. The data was averaged over 30 evacuation processes. The initial conditions were similar to those in Fig. 2. The initial number of pedestrians was $N = 200$. See the plot's title for the corresponding distance from the obstacles to the door. See the legend for the gap between the obstacles.

to be a velocity achievable by non-professional runners. Bear in mind that similar results can be obtained for desired velocities in the range $v_d \geq 4$ m/s, where pressure conditions become dangerous.

4.2. The two-entry vestibule

In this Section, we present and discuss the room evacuation results of a vestibule with two entries (left and right entries). The room layout is illustrated in Fig. 1a.

4.2.1. Effects of the distance and the wall friction

This section introduces the effects of the wall friction and the distance from the panels to the exit. Fig. 4a shows the evacuation flow as a function of the distance d between the panel and the exit door. Notice that the pedestrian's diameter scales the horizontal axis and each curve is associated with a particular friction coefficient value κ_w .

The horizontal dashed lines stand for the evacuation flow without an obstacle. Each line corresponds to a different κ_w value; the letters 'a', 'b' and 'c' in Fig. 4a stand for $\kappa_w = 0$, and 3.05×10^5 , 3.05×10^6 respectively. The flow values associated to these κ_w are $J_a = (7.6 \pm 0.7)$ p/s, $J_b = (6.7 \pm 0.5)$ p/s and $J_c = (5.7 \pm 0.5)$ p/s. When the curves exceed the corresponding horizontal dashed lines, it means that placing the obstacle improves the evacuation performance.

The three curves exhibit similar qualitative behavior: for the lowest d values, the curves increase until reaching a maximum, then, they decrease converging to a plateau. A similar behavior was reported in Ref. [50], despite that pillar-like obstacles and spherocylinders agents were used.

Notice that each curve from Fig. 4a accomplishes a specific interval of d in which placing an obstacle produces higher evacuation flows with respect to an obstacle-free room. In other words, placing a panel-like obstacle can improve or worsen the evacuation performance depending on its precise location with respect to the exit door. For example, if $\kappa_w = 3.05 \times 10^6$ the evacuation performance is improved only for $d/Diam > 3$ (see the triangle marker curve and the ‘c’ horizontal line).

The three curves show a maximum flow value for different values of d , while increasing the friction shifts the maximum value of the flow to higher values of d (see Fig. 4a). This implies that the friction coefficient κ_w has a significant influence on the evacuation. To further inspect this phenomenon, we show in Fig. 4b the evacuation flow as a function of κ_w for three representative values of d . These values are: $d = 0.92$ m, 1.84 m, 2.76 m.

If the vestibule is narrow ($d = 0.92$ m), increasing κ_w reduces the evacuation flow because of the friction in the blocking clusters (see Section 4.2.2). For a wider vestibule ($d = 1.84$ m), increasing κ_w increases the flow because it prevents more pedestrians from accessing the vestibule (this effect is explained in detail in Section 4.2.2). If the vestibule is too wide ($d = 2.76$ m), the wall frictions’ role is almost negligible. This makes the flow remain roughly constant for all the κ_w explored values.

These novel results suggests that the dynamics of the evacuations may be strongly influenced by the surface of the walls and obstacles. This fact was previously hypothesized by Hoogendoorn and Daamen [51] but has not been tested numerically until the present research (to our knowledge).

To further understand the mechanism behind this phenomenon, we studied the flow vs. density relation (the fundamental diagram). The density was sampled on the inner vestibule and it was averaged over the evacuation time. The

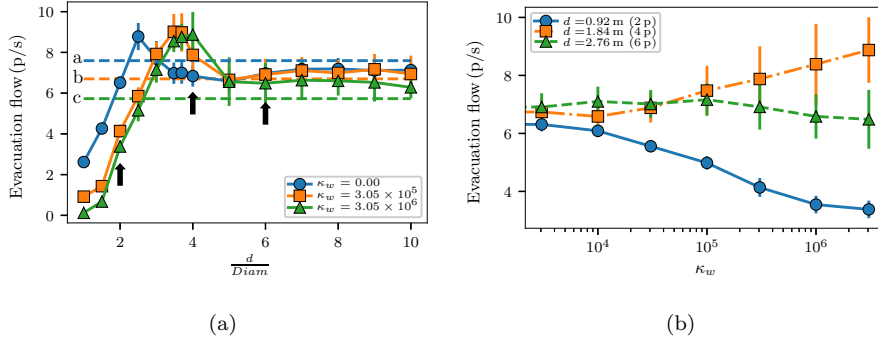


Figure 4: **(a)** Evacuation flow as a function of the distance between the panel-like obstacle and the exit door. The black arrows indicate the selected distances that were explored in Fig.4b. The horizontal axis is scaled by the pedestrian’s diameter $Diam = 0.46$ m. **(b)** Evacuation flow as a function of the wall friction coefficient. Data was averaged over 30 evacuation processes where the initial positions and velocities were random. The initial number of pedestrians was $N = 200$. The desired velocity was $v_d = 6$ m/s.

results are shown in Fig. 5 where each “subplot” is associated with a fixed value of d (see the plots’ titles). The figures are “scatter plots” where each data point belongs to a single evacuation process (with random initial conditions). The colors stand for the friction coefficient value (see the legends). The solid yellow line appearing on each plot is the average of the scattered data points.

Before focusing on each subplot in Fig. 5, we want to mention two common features common on them. The first salient feature is the negative correlation between the friction coefficient and the density (*i.e.* the higher the friction, the lower the density values; check the colors of the data points). The second feature concerns the two regimes appearing in the fundamental diagram: the free-flow regime (where increasing the density increases the flow) and the congested regime (where increasing the density reduces the flow). The situations explored in Fig. 5 display either one or both regimes depending on the value of d .

We now proceed to the analysis of each subplot. Fig. 5a corresponds to $d = 0.92$ m. Only the free-flow regime is observed for any of the κ_w values

explored. In this case, the flow does not attain the maximum because for such low-density values ($\rho < 2 \text{ p/m}^2$) there is left unused space in the vestibule. This means that more agents could potentially ingress the vestibule without producing congestion at the exit door.

The obstacle is then placed at $d = 1.38 \text{ m}$ in Fig. 5b. This situation makes it possible to observe both regimes of the fundamental diagram (the free-flow and the congested regime). We also highlight (see the shady area) that the maximum flow values correspond to intermediate densities (say, $\rho \sim 2 \text{ p/m}^2$).

Figs. 5c and 5d stand for $d = 1.84 \text{ m}$ and $d = 2.76 \text{ m}$, respectively. Under these conditions, only the congested regime is observed. In other words, the entries to the vestibule are so large that the agents have almost no impediment to access the vestibule, which ultimately congests the area close to the door.

The four plots exhibit a clear relationship between the density and the flow. If the density is very low (say, $\rho < 1.5 \text{ p/m}^2$) or very high (say, $\rho > 3 \text{ p/m}^2$), the flow will not attain its maximum value. On the other hand, intermediate values for the density (say, $\rho \sim 2 \text{ p/m}^2$) maximize the evacuation flow because there is neither congestion nor left unused space in the vestibule; see the shady areas from Fig. 5b and 5c.

The results shown in Fig. 5 indicate that too low density (or too high) lead to a suboptimal situation with a somewhat reduced flow. Therefore, we claim that the best evacuation performance is achieved with intermediate density values. This is not in complete agreement with Refs. [11, 14] where the authors suggest only a density reduction in the area close to the door. Thus, we suggest taking care of the obstacle distance and friction, in order to keep the vestibule density under control.

We emphasize that the density can either be controlled with κ_w and d , while

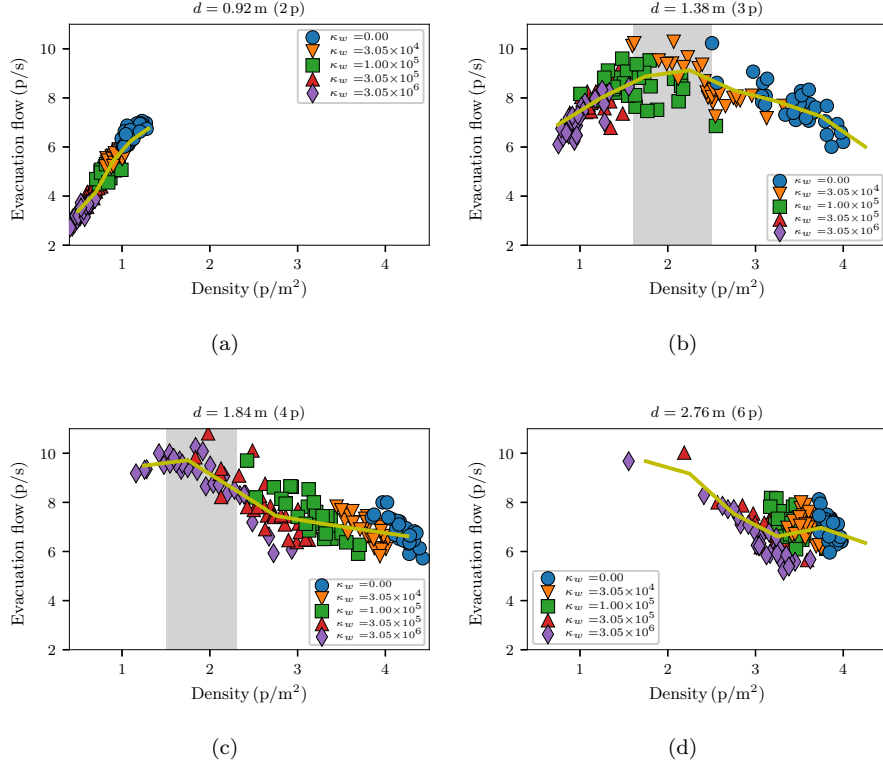


Figure 5: Evacuation flow as a function of the density (fundamental diagram) for a two-entry vestibule. The density was measured on the inner vestibule and it was averaged over the evacuation time. There are 30 data points for each friction value. Each data point belongs to a different evacuation process where the initial condition (positions and velocities) were random. The initial number of pedestrians was $N = 200$. The desired velocity was $v_d = 6$ m/s. See the plot's title for the corresponding distance from the obstacle to the door. The shady area highlights the densities that produce the maximum flow.

the vestibule density determines the evacuation flow. Consequently, the evacuation flow can be ultimately optimized by adjusting κ_w and d for a given value of v_d .

Other researchers argue that the speed (hence the flow) is not uniquely determined by the density [52]; thus, they introduce the kinetic stress observable in order to complete the description of the evacuation performance. In our research, however, it is unnecessary to include additional observables since the density measured on the inner vestibule is enough to determine the evacuation flow, at least in the context of the social force model.

As it was mentioned above that, for a given v_d , the parameters κ_w and d control the density in the inner vestibule. This phenomenon is more clearly depicted in Fig. 6 where we show the density as a function of κ_w for different d values. Increasing κ_w diminishes the density because pedestrians get stuck in the zones previous to the vestibule, which alleviates the congestion close to the exit door. This phenomenon will be further explained in the following Section.

In the same way, we observe in Fig. 6 that reducing the distance between the obstacle and the door diminishes the density too. This phenomenon occurs because the vestibule entrance is smaller (which makes it more difficult for the pedestrians to access the vestibule). Thus, it is possible to reduce the density close to the exit door by either increasing κ_w or reducing d since both effects make it more difficult for pedestrians to enter the vestibule.

Although the results shown in Fig. 6 correspond to a non-stationary situation, where the number of agents decreases over time, we show in Appendix B that the same results can be achieved in a stationary regime.

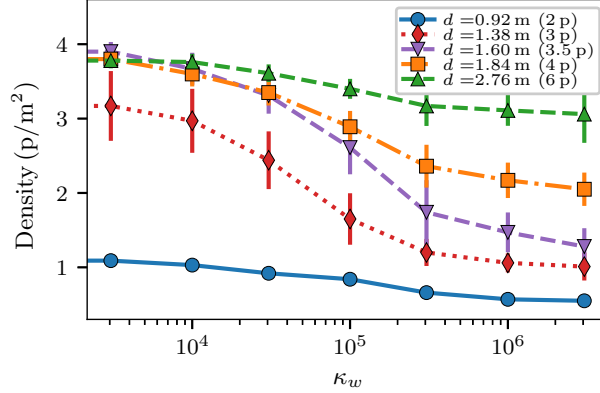


Figure 6: Density as a function of the friction coefficient. The density was measured on the inner vestibule and, it was averaged over the evacuation time until 90% of individuals evacuated. The measurements were averaged over 30 evacuation processes, while the initial conditions (position and velocity) were random. The initial number of pedestrians was $N = 200$. The desired velocity was $v_d = 6$ m/s. See the plot’s legend for the corresponding distance from the obstacle to the door.

4.2.2. The role of the blocking clusters

We previously showed that the density of the inner vestibule can be regulated by κ_w and d , while the evacuation flow depends on the density of the inner vestibule for a given v_d . The remaining question is, how do κ_w and d control the density. To answer this question, we studied the blocking clusters formed at the vestibule’s entrances. Remember that the blocking clusters are clusters of pedestrians that block a door (in this case, we consider the doors as the two entries to the vestibule). See the Section 2.2 for a formal definition of blocking cluster.

Fig. 7a shows the probability of attaining a blocking cluster in the pre-vestibule zone as a function of κ_w for different d values. The pre-vestibule zone is the area before the entrance to the vestibule. Recall that the probability was defined as the fraction of time attaining blocking clusters over the total evacuation time. In Fig. 7a we report the mean value of the blocking cluster

probability considering both entries to the vestibule.

Increasing the wall friction coefficient produces more persistent blocking clusters. This phenomenon can be noticed from the monotonically increasing behavior of the curves from Fig. 7a. In the same sense, the narrower the entries to the vestibule, the higher the blocking cluster probability. This effect is also carefully analyzed in Ref. [44] for the regular bottleneck case.

In summary, we found that increasing κ_w or reducing d produces an increment in the blocking cluster probability. The blocking cluster probability has a notorious impact on the vestibule density because it prevents pedestrians from entering the vestibule. The more blocking clusters present at the entrance of the vestibule, the less density the vestibule has, as shown in Fig. 7. In other words, the blocking clusters before the vestibule affect the density, and hence, the outgoing flow.

We may summarize our results from this Section as follows. We found that the wall friction coefficient κ_w and the distance between the obstacle and the door d affect the vestibule density. The mechanism behind this involves the “pre-vestibule” blocking clusters (say, slowing down the access to the vestibule). Additionally, we showed that the inner vestibule density has a well established relationship with the evacuation flow (expressed through the fundamental diagram). The maximum flow occurs for intermediate values of density ($\rho \sim 2$ p/m²). We stress that if the density is very high or very low, the evacuation flow is suboptimal; but it was found that the presence of the vestibule clearly enhances the evacuation for rather high values of v_d which can be related to stressful situations in which pedestrians can suffer considerable damage.

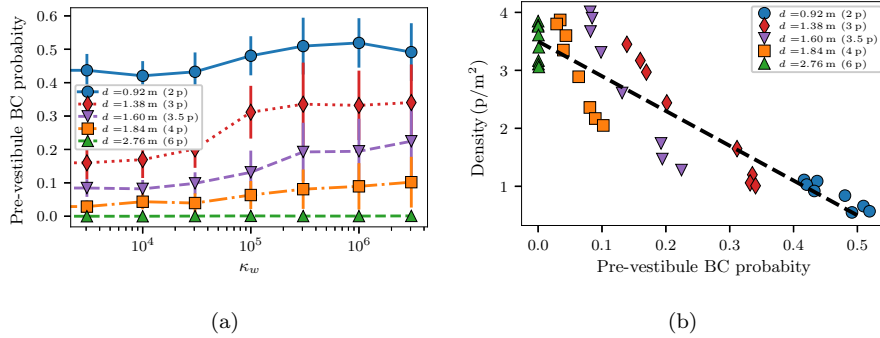


Figure 7: **(a)** Pre-vestibule blocking clusters probability as a function of the wall friction coefficient. The pre-vestibule blocking clusters is the mean value of the blocking cluster’s probability taking into account the two entries to the vestibule. **(b)** Inner vestibule density as a function of the pre-vestibule blocking cluster probability. Each point corresponds to a different friction value. The dashed line is a visual guide to see the decreasing trend. The measurements were averaged over 30 evacuation processes for random initial conditions (position and velocity). The initial number of pedestrians was $N = 200$. The desired velocity was $v_d = 6$ m/s. See the plot’s legends for the corresponding distance of the obstacle to the door.

4.3. The three-entry vestibule

The previous Section dealt with evacuations in the presence of two-entry vestibule structures. The two-entry vestibule was designed by placing a single panel-like obstacle in front of the door. As a first step towards the analysis of more complex structures, we studied the evacuations through a three-entry vestibule structure designed from two panel-like obstacles (as illustrated in Fig. 1b). The desired velocity of the agents was set to $v_d = 6$ m/s.

The previous results showed that the vestibule’s density (hence the evacuation flow) can be controlled by κ_w and d . In this sense, the gap between the two panels introduces a new parameter capable of regulating the density. Notice that the gap works as a “middle entry” to the vestibule. We intentionally choose a highly symmetric configuration in order to avoid path differences [2].

In this part of the investigation, we fix κ_w and v_d to focus only on the effect of the *gap* between panels and the distance between the panels and the exit door d . Fig. 8 shows fundamental diagrams (flow vs. density) for three representative d values ($d = 0.92$ m, 1.38 m, 1.84 m), where each plot is associated with a fix value of d (see the title of the plots). We calculated the density and the evacuation flow following the same criteria as in the previous Section. Each dot in the plots corresponds to a single evacuation process (with random initial conditions).

Fig. 8a displays the results for $d = 0.92$ m, the marker colors stand for the different *gap* between panels. Notice that distinct values of the gap produce well distinguishable density intervals. For example, $gap = 0$ p produces densities below $\rho < 1$ p/m², while $gap = 5$ p produces densities within the interval 2.5 p/m² $< \rho \leq 3.0$ p/m². It is worth mentioning that Fig. 8a only attains the free-flow regime of the fundamental diagram (say, the higher the density, the higher the flow).

Fig. 8b stands for $d = 1.38$ m. Now, the two regimes of the fundamental diagram are present (the free-flow and the congested regime) depending on the *gap* value. If $gap = 5$ p, only the congested regime is observed, meaning that the agents can easily overcrowd the vestibule. Notice that placing the obstacles at $d = 1.38$ m produces more scattered results than placing the obstacle at $d = 0.92$ m. Nevertheless, it is still possible to associate different *gap* values with well-distinguishable density values.

If the distance between panels and the exit door is $d = 1.84$ m (Fig. 8c), the optimal evacuation flow can never be achieved because the density is too high, regardless of the *gap* value. This phenomenon occurs because the left and right entries to the vestibule are large enough to simultaneously facilitate the access of many agents, leading to congestion in the vestibule structure. Under this condition, the data points are even more scattered than in the previous results,

making it more difficult to relate univocally the gap values with the vestibule density.

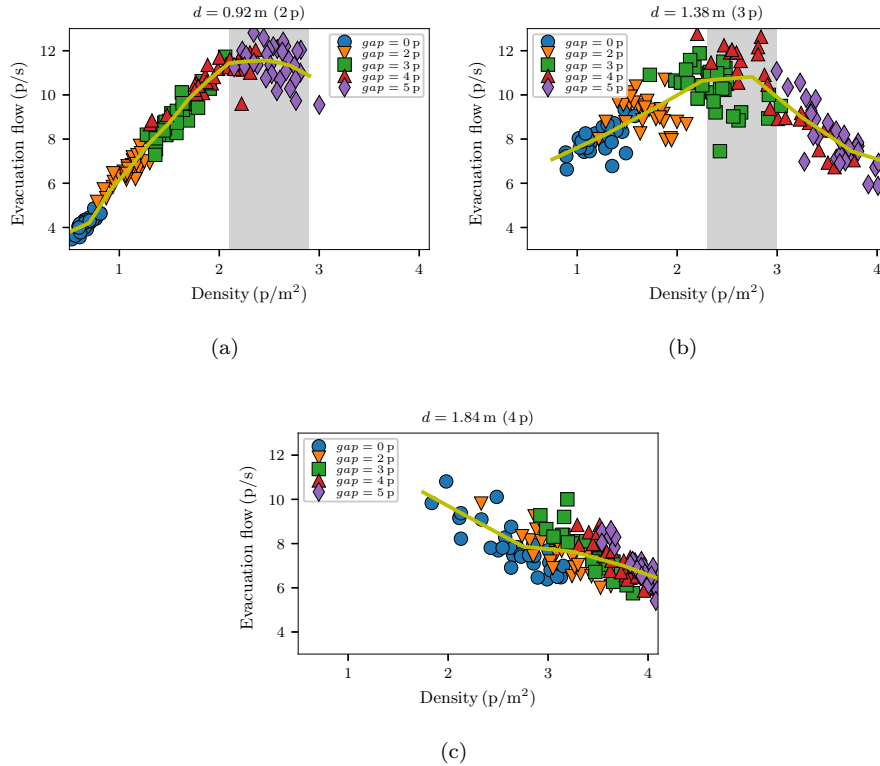


Figure 8: Evacuation flow as a function of the density (fundamental diagram) for a three-entry vestibule (see Fig. 1 for the scheme). The density was sampled on the inner vestibule and it was averaged over the evacuation time. There are 30 data points for each gap value. Each data point corresponds to a different evacuation process with random initial conditions. The initial number of pedestrians was $N = 200$. The yellow line means the average over the data points. The desired velocity was $v_d = 6 \text{ m/s}$. See the plot's title for the corresponding distance from the obstacle to the door. The shady area highlights the densities that produce the maximum flow.

The results corresponding to the three-entry vestibule share some similarities with the results of the two-entry vestibule. In both cases, the optimal flow is attained for intermediate density values ($\rho \sim 2 \text{ p/m}^2$); compare, for in-

stance, the shaded areas from Figs. 5b, 5c and 8a, 8b. If the density is too high, in all the cases, it leads to a congested regime producing a suboptimal evacuation flow. If the density is too low, the flow is also below the optimal condition.

Beyond the similarities, it should be noted that the three-entry vestibule yields a maximum flow ($J \sim 11$ p/s) that is higher than the maximum flow attained with the two-entry vestibule ($J \sim 8$ p/s), see Tables A.1 and A.2 for details. This can be explained as follows, the two entries yield a suboptimal evacuation flow because there is space left inside the vestibule. The entry in the middle, however, increases the density driving the system to the optimal flow. This phenomenon could also be obtained with multiple entries.

Besides examining the evacuation flow, we briefly explored the pressure acting on pedestrians during the evacuation process. We calculated the fraction of agents that withstand fatal pressures according to the criteria introduced in Ref. [53]. We found that the vestibule reduces the fraction of agents exposed to dangerous pressures. This promising effect is more noticeable in three-entry vestibules. Further research should be conducted to analyze the role of hazardous pressures in evacuations with vestibule structures.

The final conclusion from this Section is that the gap between two panels can be used as an effective way to regulate the density in the vestibule and therefore maximize the evacuation flow. This result promotes creating novel architectural designs that can induce better evacuation performance in a panic situation. We stress, however, that we are in no way suggesting replacing the crowd management personnel or signals systems but instead examine the results shown in this paper as an architectural improvement for pedestrian evacuations.

5. Conclusions

Placing a panel-like obstacle in front of an exit door creates a vestibule structure that enhances the evacuation performance for intermediate door-obstacle distances ($d \sim 3p$). Our investigation examined the effects of placing a two-entry vestibule (designed with only one panel-like obstacle) and a three-entry vestibule (designed with two aligned panel-like obstacles).

In both cases, we find that the density inside the vestibule uniquely determines the evacuation flow. If the vestibule gets jammed, the flow is diminished. If the density is too low, the flow is also in a suboptimal situation since there is unused space left in the vestibule. That is, more pedestrians could potentially enter the vestibule without producing congestion at the exit door. On the other hand, intermediate density values ($\rho \sim 2p/m^2$) maximize the evacuation flow. This result holds for all the explored conditions in this work.

Our main conclusion is that at least three parameters are useful for regulating the density inside the vestibule (and therefore the evacuation flow). These parameters are the wall friction coefficient κ_w , the distance between the panel and the exit door d and the gap between the two panels (in the case of a three-entry vestibule). It is worth mentioning that these parameters are architectural features that can be easily managed by designers and contractors.

Reducing d or increasing κ_w diminishes the density on the vestibule. This phenomenon is explained by means of the blocking clusters that appear at the vestibule entries. These blocking clusters limit the regular access to the vestibule. Likewise, reducing the gap between the two panels diminishes the density too.

We emphasize that the three-entry vestibule yields a maximum flow ($J \sim 11p/s$) that is higher than the maximum flow attained with the two-entry

vestibule ($J \sim 8$ p/s) and even much higher than the flow produced by a regular bottleneck without a vestibule ($J \sim 7$ p/s). This result suggests that the three-entry vestibule structure could considerably improve emergency evacuations.

As a final remark, we would like to mention that in real-life emergency evacuations, individuals may not adopt a polite behavior in order to evacuate the building. It is therefore essential to design buildings that are “panic-proof”. This means, buildings that could facilitate good evacuations even in the worst-case scenario where all the pedestrians try to escape selfishly. In this sense, we believe that finding the optimal vestibule structure is a step forward in the search for better human evacuations.

Acknowledgments

This work was supported by the National Scientific and Technical Research Council (spanish: Consejo Nacional de Investigaciones Científicas y Técnicas - CONICET, Argentina) grant Programación Científica 2019 (UBACYT) Number 2019-2019-01994.

G.A Frank thanks Universidad Tecnológica Nacional (UTN) for partial support through Grant PID Number SIUTNBA0006595.

Appendix A. Flow-density quantitative results

In this appendix, we provide a summary of the numerical results for the flow and the density. All the results are presented in two tables that exhibit the mean values and standard deviations. Tab. A.1 corresponds to the two-entry vestibule while Tab. A.2 corresponds to the three-entry vestibule.

Two-entry vestibule

d (m)	κ_w	$\langle J \rangle$ (p/s)	σ_J (p/s)	$\langle \rho \rangle$ (p/m ²)	σ_ρ (p/m ²)
0.92	0	6.5	0.3	1.10	0.08
0.92	3.05×10^4	5.5	0.2	0.92	0.06
0.92	1.00×10^5	4.9	0.2	0.83	0.06
0.92	3.05×10^5	4.1	0.3	0.66	0.07
0.92	3.05×10^6	3.3	0.3	0.54	0.06
1.38	0	7.6	0.8	3.44	0.38
1.38	3.05×10^4	8.5	0.8	2.44	0.39
1.38	1.00×10^5	8.4	0.6	1.64	0.35
1.38	3.05×10^5	7.9	0.6	1.19	0.18
1.38	3.05×10^6	7.1	0.6	1.00	0.19
1.84	0	6.8	0.5	4.18	0.14
1.84	3.05×10^4	6.8	0.5	3.79	0.16
1.84	1.00×10^5	7.4	0.8	3.16	0.30
1.84	3.05×10^5	7.8	1.1	2.64	0.35
1.84	3.05×10^6	8.8	1.1	1.93	0.45
2.76	0	6.9	0.4	3.84	0.07
2.76	3.05×10^4	7.0	0.4	3.60	0.12
2.76	1.00×10^5	7.1	0.5	3.39	0.13
2.76	3.05×10^5	6.9	0.7	3.17	0.27
2.76	3.05×10^6	6.4	1.0	3.05	0.39

Table A.1: Mean value and standard deviation of the flow (J) and the density (ρ) for different d and κ_w . The desired velocity was $v_d = 6$ m/s.

Three-entry vestibule

d (m)	gap (p)	$\langle J \rangle$ (p/s)	σ_J (p/s)	$\langle \rho \rangle$ (p/m ²)	σ_ρ (p/m ²)
0.92	0	4.1	0.3	0.66	0.07
0.92	2	6.6	0.6	1.10	0.14
0.92	3	8.9	0.9	1.56	0.17
0.92	4	10.8	0.9	1.98	0.29
0.92	5	11.4	0.8	2.56	0.20
1.38	0	7.9	0.6	1.19	0.18
1.38	2	9.2	0.7	1.70	0.23
1.38	3	10.2	0.9	2.38	0.27
1.38	4	10.0	1.9	2.99	0.43
1.38	5	8.0	1.3	3.57	0.26
1.84	0	7.8	1.1	2.64	0.35
1.84	2	7.5	0.8	3.14	0.28
1.84	3	7.5	0.9	3.44	0.24
1.84	4	7.0	0.8	3.75	0.23
1.84	5	6.9	0.8	3.91	0.18

Table A.2: Mean value and standard deviation of the flow (J) and the density (ρ) for different d and gap . The wall friction coefficient was $\kappa_w = 3.05 \times 10^5$ and the desired velocity $v_d = 6$ m/s.

Appendix B. Density in the stationary regime

The purpose of this appendix is to show that the density measurements in the non-stationary regime are equivalent to the measurements in the stationary regime. By “stationary” we mean that the number of agents is constant in time; we achieve this by re-entering the outgoing agents in order to keep $N = 200$.

Fig. B.9 shows the density in the inner vestibule as a function of the friction coefficient for different d values. The measurements correspond to a stationary regime that lasts $\Delta t = 1000$ s. The qualitative behavior from Fig. B.9 is similar to the qualitative behavior from Fig. 6 (which corresponds to a non-stationary

situation). This means that the density dependence on κ_w and d is not an effect produced by the decreasing number of pedestrians over time.

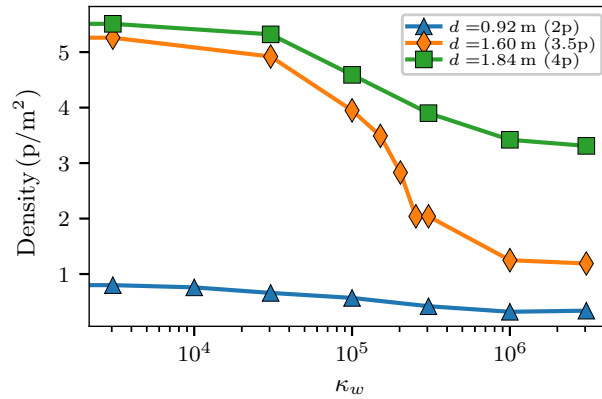


Figure B.9: Density as a function of the friction coefficient. The density was measured on the inner vestibule. The measurements are averaged over $\Delta t = 1000$ s. The number of pedestrians was $N = 200$ all the time since the outgoing agents were re-entered. The desired velocity was $v_d = 6$ m/s. See the plot’s legend for the corresponding distance from the obstacle to the door.

References

References

- [1] D. Helbing, I. Farkas, T. Vicsek, Simulating dynamical features of escape panic, *Nature* 407 (6803) (2000) 487–490.
- [2] R. Escobar, A. De La Rosa, Architectural design for the survival optimization of panicking fleeing victims, in: *European Conference on Artificial Life*, Springer, 2003, pp. 97–106.
- [3] C. M. Harris, *Dictionary of Architecture and Construction.*, McGraw-Hill, 2006.

- [4] D. Helbing, L. Buzna, A. Johansson, T. Werner, Self-organized pedestrian crowd dynamics: Experiments, simulations, and design solutions, *Transportation science* 39 (1) (2005) 1–24.
- [5] G. A. Frank, C. O. Dorso, Room evacuation in the presence of an obstacle, *Physica A: Statistical Mechanics and its Applications* 390 (11) (2011) 2135–2145.
- [6] I. Zuriguel, I. Echeverria, D. Maza, R. C. Hidalgo, C. Martín-Gómez, A. Garcimartín, Contact forces and dynamics of pedestrians evacuating a room: the column effect, *Safety science* 121 (2020) 394–402.
- [7] Á. Garcimartín, D. Maza, J. M. Pastor, D. R. Parisi, C. Martín-Gómez, I. Zuriguel, Redefining the role of obstacles in pedestrian evacuation, *New Journal of Physics* 20 (12) (2018) 123025.
- [8] X. Shi, Z. Ye, N. Shiwakoti, D. Tang, J. Lin, Examining effect of architectural adjustment on pedestrian crowd flow at bottleneck, *Physica A: Statistical Mechanics and its Applications* 522 (2019) 350–364.
- [9] Y. Liu, X. Shi, Z. Ye, N. Shiwakoti, J. Lin, Controlled experiments to examine different exit designs on crowd evacuation dynamics, in: *CICTP 2016*, 2016, pp. 779–790.
- [10] N. Shiwakoti, M. Sarvi, Enhancing the panic escape of crowd through architectural design, *Transportation research part C: emerging technologies* 37 (2013) 260–267.
- [11] Y. Zhao, M. Li, X. Lu, L. Tian, Z. Yu, K. Huang, Y. Wang, T. Li, Optimal layout design of obstacles for panic evacuation using differential evolution, *Physica A: Statistical Mechanics and its Applications* 465 (2017) 175–194.
- [12] Q. Li, Y. Gao, L. Chen, Z. Kang, Emergency evacuation with incomplete information in the presence of obstacles, *Physica A: Statistical Mechanics and its Applications* 533 (2019) 122068.

- [13] M. Haghani, M. Sarvi, Simulating pedestrian flow through narrow exits, *Physics Letters A* 383 (2-3) (2019) 110–120.
- [14] Y. Zhao, T. Lu, L. Fu, P. Wu, M. Li, Experimental verification of escape efficiency enhancement by the presence of obstacles, *Safety science* 122 (2020) 104517.
- [15] Z. Ding, Z. Shen, N. Guo, K. Zhu, J. Long, Evacuation through area with obstacle that can be stepped over: experimental study, *Journal of Statistical Mechanics: Theory and Experiment* 2020 (2) (2020) 023404.
- [16] A. Kirchner, K. Nishinari, A. Schadschneider, Friction effects and clogging in a cellular automaton model for pedestrian dynamics, *Physical review E* 67 (5) (2003) 056122.
- [17] D. Yanagisawa, R. Nishi, A. Tomoeda, K. Ohtsuka, A. Kimura, Y. Suma, K. Nishinari, Study on efficiency of evacuation with an obstacle on hexagonal cell space, *SICE Journal of Control, Measurement, and System Integration* 3 (6) (2010) 395–401.
- [18] T. Matsuoka, A. Tomoeda, M. Iwamoto, K. Suzuno, D. Ueyama, Effects of an obstacle position for pedestrian evacuation: Sf model approach, in: *Traffic and Granular Flow'13*, Springer, 2015, pp. 163–170.
- [19] N. Shiwakoti, X. Shi, Z. Ye, A review on the performance of an obstacle near an exit on pedestrian crowd evacuation, *Safety science* 113 (2019) 54–67.
- [20] I. Zuriguel, A. Janda, A. Garcimartín, C. Lozano, R. Arévalo, D. Maza, Silo clogging reduction by the presence of an obstacle, *Physical review letters* 107 (27) (2011) 278001.
- [21] C. Lozano, A. Janda, A. Garcimartin, D. Maza, I. Zuriguel, Flow and clogging in a silo with an obstacle above the orifice, *Physical Review E* 86 (3) (2012) 031306.

- [22] F. Alonso-Marroquin, S. Azeezullah, S. Galindo-Torres, L. Olsen-Kettle, Bottlenecks in granular flow: when does an obstacle increase the flow rate in an hourglass?, *Physical Review E* 85 (2) (2012) 020301.
- [23] N. Shiwakoti, M. Sarvi, G. Rose, M. Burd, Enhancing the safety of pedestrians during emergency egress: can we learn from biological entities?, *Transportation research record* 2137 (1) (2009) 31–37.
- [24] A. Garcimartín, J. Pastor, L. Ferrer, J. Ramos, C. Martín-Gómez, I. Zuriguel, Flow and clogging of a sheep herd passing through a bottleneck, *Physical Review E* 91 (2) (2015) 022808.
- [25] I. Zuriguel, J. Olivares, J. M. Pastor, C. Martín-Gómez, L. M. Ferrer, J. J. Ramos, A. Garcimartín, Effect of obstacle position in the flow of sheep through a narrow door, *Physical Review E* 94 (3) (2016) 032302.
- [26] A. Seyfried, B. Steffen, W. Klingsch, M. Boltes, The fundamental diagram of pedestrian movement revisited, *Journal of Statistical Mechanics: Theory and Experiment* 2005 (10) (2005) P10002.
- [27] X. Ren, J. Zhang, W. Song, Flows of walking and running pedestrians in a corridor through exits of different widths, *Safety Science* 133 (2021) 105040.
- [28] S. Cao, A. Seyfried, J. Zhang, S. Holl, W. Song, Fundamental diagrams for multidirectional pedestrian flows, *Journal of Statistical Mechanics: Theory and Experiment* 2017 (3) (2017) 033404.
- [29] D. Helbing, A. Johansson, H. Z. Al-Abideen, Dynamics of crowd disasters: An empirical study, *Physical review E* 75 (4) (2007) 046109.
- [30] R. Lohner, B. Muhamad, P. Dambalmath, E. Haug, Fundamental diagrams for specific very high density crowds, *Collective Dynamics* 2 (2018) 1–15.
- [31] T. Kretz, An overview of fundamental diagrams of pedestrian dynamics.

- [32] L. D. Vanumu, K. R. Rao, G. Tiwari, Fundamental diagrams of pedestrian flow characteristics: A review, *European transport research review* 9 (4) (2017) 49.
- [33] S. Cao, L. Lian, M. Chen, M. Yao, W. Song, Z. Fang, Investigation of difference of fundamental diagrams in pedestrian flow, *Physica A: Statistical Mechanics and its Applications* 506 (2018) 661–670.
- [34] A. Nicolas, S. Bouzat, M. N. Kuperman, Pedestrian flows through a narrow doorway: Effect of individual behaviours on the global flow and microscopic dynamics, *Transportation Research Part B: Methodological* 99 (2017) 30–43.
- [35] G. Bernardini, E. Quagliarini, M. D’Orazio, Towards creating a combined database for earthquake pedestrians’ evacuation models, *Safety science* 82 (2016) 77–94.
- [36] W. Daamen, S. P. Hoogendoorn, P. H. Bovy, First-order pedestrian traffic flow theory, *Transportation research record* 1934 (1) (2005) 43–52.
- [37] A. Seyfried, O. Passon, B. Steffen, M. Boltes, T. Rupperecht, W. Klingsch, New insights into pedestrian flow through bottlenecks, *Transportation Science* 43 (3) (2009) 395–406.
- [38] M. Bukáček, P. Hrabák, M. Krbálek, Experimental analysis of two-dimensional pedestrian flow in front of the bottleneck, in: *Traffic and Granular Flow’13*, Springer, 2015, pp. 93–101.
- [39] A. Seyfried, M. Boltes, J. Kähler, W. Klingsch, A. Portz, T. Rupperecht, A. Schadschneider, B. Steffen, A. Winkens, Enhanced empirical data for the fundamental diagram and the flow through bottlenecks, in: *Pedestrian and Evacuation Dynamics 2008*, Springer, 2010, pp. 145–156.
- [40] B. Haworth, M. Usman, G. Berseth, M. Kapadia, P. Faloutsos, On density–flow relationships during crowd evacuation, *Computer Animation and Virtual Worlds* 28 (3-4) (2017) e1783.

- [41] G. H. Risto, H. J. Herrmann, et al., Density patterns in two-dimensional hoppers, *Physical Review E* 50 (1) (1994) R5.
- [42] I. Sticco, G. Frank, C. Dorso, Social force model parameter testing and optimization using a high stress real-life situation, *Physica A: Statistical Mechanics and its Applications* 561 (2021) 125299.
- [43] A. Strachan, C. Dorso, Fragment recognition in molecular dynamics, *Physical Review C* 56 (2) (1997) 995.
- [44] D. R. Parisi, C. O. Dorso, Microscopic dynamics of pedestrian evacuation, *Physica A: Statistical Mechanics and its Applications* 354 (2005) 606–618.
- [45] I. M. Sticco, G. A. Frank, S. Cerrotta, C. O. Dorso, Room evacuation through two contiguous exits, *Physica A: Statistical Mechanics and its Applications* 474 (2017) 172–185.
- [46] F. Cornes, G. Frank, C. Dorso, Microscopic dynamics of the evacuation phenomena in the context of the social force model, *Physica A: Statistical Mechanics and its Applications* 125744.
- [47] D. Littlefield, *Metric handbook*, Routledge, 2008.
- [48] J.-B. Morin, M. Bourdin, P. Edouard, N. Peyrot, P. Samozino, J.-R. Lacour, Mechanical determinants of 100-m sprint running performance, *European journal of applied physiology* 112 (11) (2012) 3921–3930.
- [49] S. Plimpton, Fast parallel algorithms for short-range molecular dynamics, *Journal of computational physics* 117 (1) (1995) 1–19.
- [50] I. Echeverría-Huarte, I. Zuriguel, R. Hidalgo, Pedestrian evacuation simulation in the presence of an obstacle using self-propelled spherocylinders, *Physical Review E* 102 (1) (2020) 012907.
- [51] S. P. Hoogendoorn, W. Daamen, Pedestrian behavior at bottlenecks, *Transportation science* 39 (2) (2005) 147–159.

- [52] A. Garcimartín, J. M. Pastor, C. Martín-Gómez, D. Parisi, I. Zuriguel, Pedestrian collective motion in competitive room evacuation, *Scientific reports* 7 (1) (2017) 1–9.
- [53] F. E. Cornes, G. A. Frank, C. O. Dorso, High pressures in room evacuation processes and a first approach to the dynamics around unconscious pedestrians, *Physica A: Statistical Mechanics and its Applications* 484 (2017) 282–298.